Soft Matter

Effects of Strain-dependent Surface Stress on the Adhesive Contact of a Rigid Sphere to a Compliant Substrate

Journal:	*Soft Matter*
Manuscript ID	SM-ART-12-2018-002579.R1
Article Type:	Paper
Date Submitted by the Author:	31-Jan-2019
Complete List of Authors:	Liu, Zezhou; Cornell University, Department of Mechanical and Aerospace Engineering Jensen, Katharine; Williams College, Physics Xu, Qin; ETH Zurich, Department of Materials Style, Robert; ETH Zurich, Department of Materials Dufresne, Eric; Eidgenossische Technische Hochschule Zurich Departement fur Materialwissenschaft Jagota, Anand; Lehigh University, Department of Chemical Engineering Hui, Chung-Yuen; Cornell University, Theoretical and Applied Mechanics

Effects of Strain-dependent Surface Stress on the Adhesive Contact of a Rigid Sphere to a Compliant Substrate

Zezhou Liu[1], Katharine E. Jensen[2], Qin Xu[3], Robert W. Style[3], Eric R. Dufresne[3], Anand Jagota[4] and Chung-Yuen Hui[*1]

[1] Department of Mechanical & Aerospace Engineering, Field of Theoretical and Applied Mechanics, Cornell University, Ithaca, NY 14853, USA

[2] Department of Physics, Williams College, Williamstown, MA 01267, USA

[3] Department of Materials, ETH Zürich, Zürich, Switzerland.

[4] Department of Chemical & Biomolecular Engineering and Bioengineering Program, 111 Research Drive, Lehigh University, Bethlehem, PA 18015, USA.

[*] Corresponding Author, ch45@cornell.edu

Abstract:

Recent experiments have reported that the surface stress of soft elastic solids can increase rapidly with surface strain. For example, when a small hard sphere in adhesive contact with a soft silicone gel is slowly retracted from its rest position, it was found that the retraction force versus displacement relation cannot be explained either by the Johnson-Kendall-Roberts (JKR) theory or a recent indentation theory based on an isotropic surface stress that is independent of surface strain. In this paper, we address this problem using a finite element method to simulate the retraction process. Our numerical model does not have the restrictions of the aforementioned theories; that is, it can handle large nonlinear elastic deformation as well as a surface-strain-dependent surface stress. Our simulation is in good agreement with experimental force versus displacement data with no fitting parameters. Therefore, our results lend further support to the claim that significant strain-dependent surface stresses can occur in simple soft elastic gels. However, significant challenges remain in the reconciliation of theory and experiments, particularly regarding the geometry of the contact and substrate deformation.

1 Introduction

The importance of *surface energy* in surface science is well established. However, a closely related but physically *different* quantity, *surface stress*, is often neglected for solids. Its effects are felt over a characteristic length scale, the *elastocapillary length*, σ/E, where E is the Young modulus and σ the magnitude of the surface stress. For conventional stiff materials (metals and ceramics) its value is generally immeasurably small.[1–4] However, elastomers, gels, biomaterials, and materials commonly used in biomimetics are often very soft in comparison. For these solids, the elastocapillary length can be tens of microns or larger. This brings about a wide range of interesting mechanical phenomena and properties. For example, surface stresses can flatten or round off solid surfaces by deformation.[5–8] Soft gel surfaces can resist indention by surface stresses rather than by bulk elasticity.[9–11] The Hertz and Johnson-Kendall-Roberts (JKR) theories for adhesionless and adhesive contact,[12] respectively, which are widely used to interpret indentation data, are no longer applicable for soft solids and have to be reformulated.[10,11,13–16] The contact angle in partial wetting is no longer governed by Young's equation – it depends on the surface stress of the solid substrate as well as its elasticity.[14,17–20] The deflection of thin films of

relative stiff materials can be substantially affected by surface stress of the film and it is possible to exploit this phenomenon to measure solid surface stress.[21–25] Composites with liquid inclusions can be stiffened by interfacial tension.[26]

However, the intensely investigated role of surface stress addresses only the simplest constitutive behavior that a soft solid surface can have. The majority of work reported so far for soft solids takes the influence of the surface to be represented by an isotropic, homogeneous, and strain-independent residual stress.[3] This is a natural approach since most of the soft solids used in these experiments are gels and elastomers with a large solvent component, which leads to the expectation that the surface stress would behave similar to that of liquids. However, it has long been theorized that solid surface stress can be strain-dependent.[27–29] Indeed, Gurtin and Murdoch[30] raised the question of whether solid surfaces possess elasticity (surface Lame' constants) in addition to a residual surface stress and this has recently been demonstrated experimentally.[25,31,32] However, there is still some controversy on certain aspects of these findings since the surface elastic constants measured in these experiments are surprisingly high. For example, Xu et al.[31] reported that the surface bulk modulus of silicone gel is about six times the surface tension at zero surface strain.

Of particular interest to us are the recent experiments by Jensen et al.[32] which lend further support to this extraordinarily high strain-dependent surface stress of silicone gels. To put this into perspective, let us begin by reviewing their experiments and approach to data interpretation. The experiment begins by moving a hard sphere (silica bead) into contact with a silicone gel substrate at the vertical position $D = 0$, as shown in Fig. 1(a), where D is the vertical distance between the bottom of the sphere and the undeformed position of the silicone gel surface. Due to adhesion, a tension force, F_0, is required to hold the sphere at $D = 0$. The sphere is then retracted slowly (Fig. 1(b)) until final detachment between the sphere and gel. During retraction, the force on the load cell F increases. During most of the experiment, the contact line shrinks little until some critical displacement, after which the contact line retracts rapidly and detachment occurs. The dynamics during the detachment was recently studied by Berman et al.[33]; here we focus on the force-displacement relation before detachment.

Two theories were proposed to explain the force-displacement (*F vs D*) data from initial contact through final detachment: the extended JKR theory of Maugis[34] and a standard capillary theory based on a constant surface-strain-independent isotropic surface stress.[13] Specifically, the force versus *D* relations predicted by these theories are:

$$F^{\text{Maugis}} = -\frac{3aK}{2}\left(-D - \frac{R}{2} + \frac{R^2 - a^2}{4a}\ln\frac{R+a}{R-a}\right), \quad \frac{1}{K} = \frac{3}{4}\left(\frac{1-\nu^2}{E}\right) \tag{1}$$

and

$$F^{\text{fluid}} = 2\pi\sigma\frac{a^2}{R}, \tag{2}$$

where E is Young's modulus of the gel, ν is the Poisson's ratio, R is the radius of the sphere, a is the contact radius, and σ is the magnitude of the surface stress. From their experiments, E=5.6 kPa, $\nu = 0.48$, and R ranges from about 9 to 20 μm, σ is taken to be 20 mN/m, and the initial contact radius $a = a_0$ is obtained from experiments. Thus, the elasto-capillary number $\sigma_0 / \mu R$ lies between 0.18 to 0.4. However, both theories failed to explain experimental data.

The failure of these theories is not difficult to understand. Maugis's theory does not account for the fact that surface stresses can resist deformation. In addition, it is not valid for large deformation. Here we note that the

maximum displacement in the experiments can easily exceed the radius of the sphere, so linear elasticity theory is not expected to work. Although Maugis used an exact sphere indenter profile instead of a paraboloid, his analysis is still based on approximating the indenter as an elastic half space, and small strain linear elasticity theory is used throughout his analysis. Hence, the errors under large deformation are expected to be of the same order as the JKR theory. Indeed, Lin et al.[35] have shown that, in the absence of surface stresses, the JKR theory is more accurate than Maugis's theory for indentation depth less than the radius of the sphere. Beyond that, both JKR and Maugis theories both break down.

The capillary theory fails because it is based on the assumption that surface stresses is a constant, independent of surface strain; it does not account for substrate elasticity – the gel is treated as a simple fluid with no shear modulus. However, recent experiments[25,31,32] on the same and similar gel systems showed that surface stresses increase rapidly with surface strain, i.e., using a constant surface stress in eq. (2) will underestimate the force, which is indeed the case.

Jensen et al.[32] observed that the silicone meniscus below the sphere resembles a liquid capillary bridge that can be fitted by an axisymmetric surface with a *constant mean curvature* starting from the contact line (red curve in Fig. 1(b)). They quantified the size of this constant mean curvature region, ΔS, by measuring the arc length along the surface profile from the contact line to the place where it deviates from the experimental data. They found that ΔS grows exponentially with the imposed displacement D, and used ΔS as a measure of the elastocapillary length, with the magnitude of the surface stress at a given displacement D assumed to be given by

$$\sigma(D) = \sigma_0 \Delta S(D) / \Delta S_0, \tag{3}$$

where ΔS_0 is the value of ΔS at F_0 or at $D = 0$. Next, they replaced the constant surface tension σ in eq. (2) by $\sigma(D)$ in eq. (3) and assumed that the elastic and surface stress contribution to the external force is given by (1) and (2) respectively. By adding these two contributions they were able to explain their force versus displacement data. The increase in the magnitude of the surface stress with surface strain is found to be consistent with Xu et al.[31]

The obvious difficulties with this approach are:

(i) There is no rigorous justification for (3);

(ii) Superposition is not valid for large deformation, thus the force contributions from elasticity and surface stress (whether strain-independent or strain-dependent) may not be simply summed;

(iii) The assumption of strain-dependent surface stress is inconsistent with capillary theory, that is, eq. (2) is valid only if the surface stress is a constant. Indeed, consider the curve in the *r-z* plane of an axisymmetric surface (solid blue line in Fig. 2). We parametrize this curve by its arc length *s*, and denote the unit tangent, binormal and normal vectors by $\mathbf{t}(s), \mathbf{b}(s)$ and $\mathbf{n}(s)$ respectively. The surface stress, assumed to be isotropic (but not necessarily to be strain-independent), takes the form $\boldsymbol{\sigma} = \sigma(s)\mathbf{1}_s$, where $\boldsymbol{\sigma}$ is the true surface stress tensor, $\sigma(s)$ is the magnitude of surface stress which depends on s, and $\mathbf{1}_s$ is surface identity tensor in the deformed configuration. Static equilibrium yields[29,30,36,37]

$$\sigma_{nn}^{\text{bulk}} = \sigma(s)\kappa(s), \quad \sigma_{nt}^{\text{bulk}} = \frac{\partial \sigma(s)}{\partial s}, \tag{4}$$

where $\kappa(s)$ is two times the mean curvature of the surface, and σ_{nn}^{bulk} and σ_{nt}^{bulk} are the traction components of the traction vector $\boldsymbol{T}_{bulk} = \sigma_{nn}^{bulk}\mathbf{n}(s) + \sigma_{nt}^{bulk}\mathbf{t}(s)$ of the bulk material right underneath the surface. σ_{nn}^{bulk} and σ_{nt}^{bulk} are also known as the Laplace pressure and Marangoni stress. However, even if $\kappa(s)$ is a constant, $\sigma(s)$ varies from position to position since it is strain-dependent. Hence, σ_{nn}^{bulk} cannot be constant and $\sigma_{nt}^{bulk} \neq 0$ by eq (4), which obviously violates the hydrostatic state of stress demanded by capillary theory. In short, the change in surface stress along *s* must be balanced by shear stress exerted by the bulk, and hence a hydrostatic state of stress is impossible.

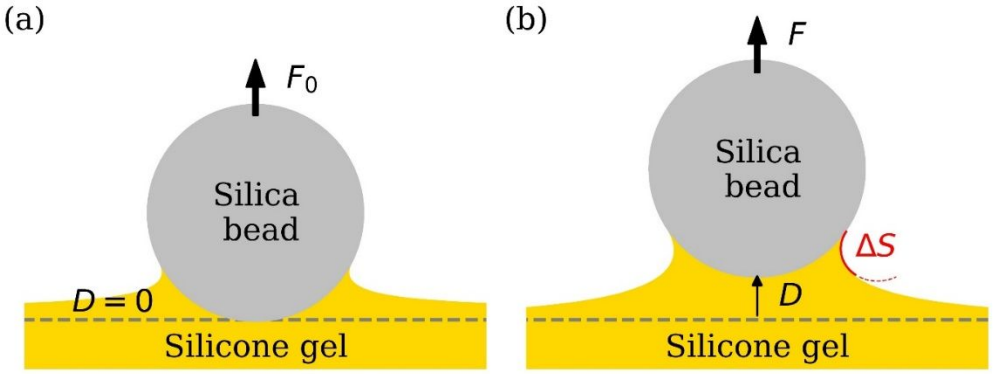

Fig. 1. Schematic of the experiment and problem statement. The dotted line indicates the position of the undeformed gel surface.

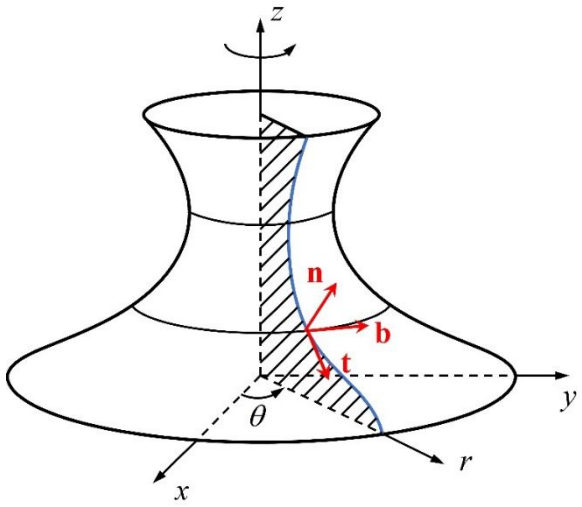

Fig. 2. Schematics of an axisymmetric surface. **n**, **t** and **b** are the unit normal, tangent and binormal vectors to the blue curve in the *r*-*z* plane of an axisymmetric surface.

2 Finite element model (FEM)

Given the above difficulties, we decided to simulate the experiment using a finite element model which allows for large deformation and strain-dependent surface stress. Specifically, we simulated the surface mechanical behavior using a strain-dependent surface stress model, i.e.,

$$\boldsymbol{\sigma} = \left[\sigma_0 + B\left(J_s - 1\right)\right]\mathbf{1}_s \tag{5}$$

where σ_0 is the magnitude of surface stress at zero surface strain, B is the surface bulk modulus, J_s is the determinant of the surface deformation gradient tensor which is the ratio of the surface area of a material element in the current and reference configurations. This constitutive model has been implemented as a new axisymmetric surface element in a FE program (ABAQUS®), and the details are provided in the Supplementary Material. Note that our surface model eq. (5) does not include shear effects which was recently discovered by Xu et al.[25] Since our problem is axisymmetric, the shear surface strain is identically zero; however, the surface stress state can now be bi-axial. We will discuss this possibility in the discussion.

The nonlinear elasticity of the substrate is assumed to be governed by a neo-Hookean incompressible solid with strain energy density function

$$W = \frac{\mu}{2}(I_1 - 3), \tag{6}$$

where I_1 is the trace of the right Cauchy-Green deformation tensor and μ is the small strain shear modulus. Due to incompressibility $\mu = E/3$. In our simulations, the material properties of the bulk and surface are given by Jensen et al, i.e., $E = 5.6$ kPa, $\sigma_0 = 20$ mN/m. The surface bulk modulus B in all simulations is taken to be $B = 6\sigma_0$, as reported by Xu et al.[31] for a similar gel. In this sense, there is no fitting parameter.

Our axisymmetric finite element model is shown schematically in Fig. 3 and implemented in the commercial FEM software, ABAQUS®. In our model, the silica sphere is modeled as an analytical rigid sphere. Also, the new user-defined strain-dependent axisymmetric surface elements are attached to the surface to model the constitutive model given by (5).

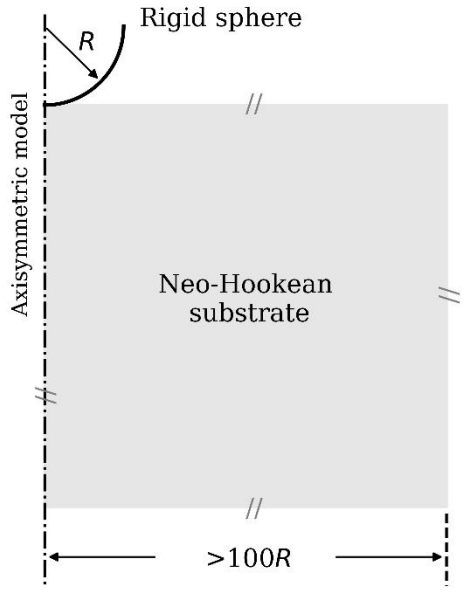

Fig. 3. Schematic of axisymmetric finite element model. The silica bead is modeled as a rigid sphere (solid black line) with radius *R*, and the elastic substrate is approximated by a sufficiently large square (shaded region) with neo-Hookean material.

Simulations are carried out using rigid sphere radii *R* (from about 9 microns to 22 microns) as employed in the experiments. The cross-section of the neo-Hookean substrate is approximated by a square with the length of 2000

microns (nearly 100 times the largest R). We verified that increasing the size of the square does not affect the FE results. On the boundaries of the axisymmetric axis (left edge) and right edge, no radial displacement (in r-direction) or shear traction is allowed; on the bottom edge, the vertical displacement (in z-direction) and shear traction are both zero; on the top boundary, the new user-defined surface elements (UEL) are used to model surface stress. On the rigid sphere, a normal displacement is prescribed in the z-direction while the radial displacement is fixed to be zero. The surface stress on the rigid body is ignored.

To simulate adhesive contact, we utilize the following loading scheme devised by Xu et al.[10] The system consisting of the rigid sphere and the neo-Hookean half-space is loaded in four steps, as illustrated in Fig. 4: (1) surface stress is applied incrementally to the surface elements until it reaches σ_0. Note in this step, there is no deformation anywhere; (2) A vertical imposed displacement is applied incrementally on the rigid sphere to push it down into the half-space, $D<0$ resulting in a finite contact radius a_0. During this process, we enforce full-friction contact. That is, there is no slip. (3) The vertical displacement then is gradually reduced to zero ($D=0$) with the contact radius held fixed; the final stage of this step corresponds to the initial state shown in Fig. 1(a). (4) We then increase the vertical displacement on the sphere gradually ($D>0$) with the contact radius *fixed* at a_0 which corresponds to Fig. 1(b). We repeat this procedure with different sphere radii R.

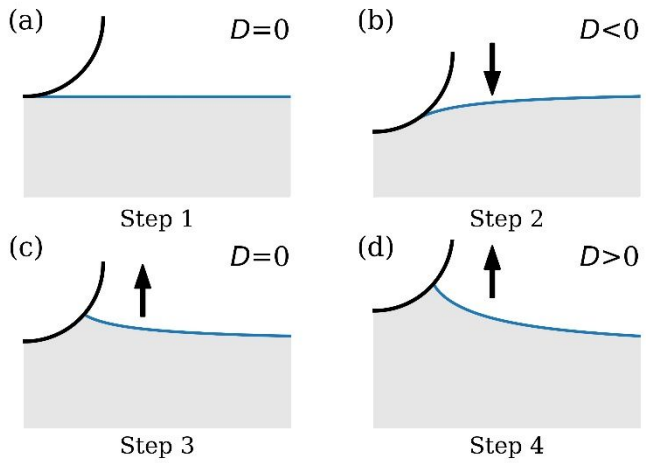

Fig. 4. Four-step load scheme in FEA. The strain-dependent surface elements (solid blue line) are attached to the surface of substrate (shaded region). (a) No deformation occurs and surface stress is incrementally applied to the value of σ_0; (b) rigid sphere (solid black line) is pushed into the substrate creating a finite contact region, with radius a_o; (c) the contact radius is fixed at a_o while the rigid sphere is pulled back to the position D=0, corresponding to the initial stage of the experiments; (d) rigid sphere is pulled upwards to D>0 to simulate the experiments.

The initial contact radius a_0 used in our simulations for different sphere radius is obtained from the supplementary information in Jensen et al. Here we note that, in experiments, the contact line slips a small amount as the sphere moves upwards. Jensen et al.[32] (SI) shows that when $D = R$, the initial contact radius decreases by about 10%. Let us denote the contact radius and displacement by a_c and D_c just before rapid shrinkage occurs, typically when F reaches its maximum value. In general, a_c and D_c depend on the radius of sphere and can be estimated from the supplementary information in Jensen et al.[32] To ensure accurate representation of experiments, in all simulations, step 4 is modified by allowing slippage of the contact line. Specifically, the contact radius a at each imposed displacement is estimated by linear interpolation between a_0 and a_c.

3 Results

3.1 Initial force F_0 versus sphere radius R

Due to adhesion, an external tensile force F_0 is required to hold the sphere at $D = 0$. In Fig. 5, we plot F_0 against sphere radius R. The experimental data of Jensen et al.[32] are plotted as symbols. The F_0 predicted using the extended JKR theory by Maugis (eq. (1)) and capillary theory (eq. (2)) are also plotted in the same figure for comparison. In addition, we also plot the analytic solution by Hui et al.[13] for the indentation problem of a rigid sphere into an elastic substrate with surface stress and adhesion (see the Electronic Supplementary Information for details). It should be noted that this solution is based on small deformation and more importantly, a *constant* surface stress, hence it will underestimate the force at a given displacement if the surface stress increases with surface strain. The procedures used to obtain this result are given in the Electronic Supplementary Information. Fig. 5 shows that the FE results impressively match the experimental data without any fitting parameters, while predictions by eqs. (1), (2) and Hui et al's theory all underestimate the force.

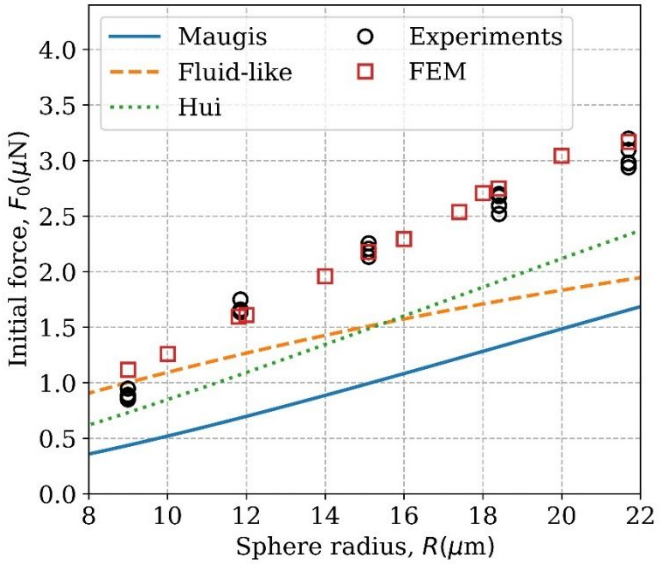

Fig. 5. Initial contact force F_0 plotted versus sphere radius R. Predictions based on the extended JKR theory by Maugis, capillary theory and analytic solution by Hui et al are plotted as solid blue, dashed orange and dotted green lines, respectively. Experimental results by are plotted as black circles, and the finite element results are plotted as red squares.

3.2 External force F versus displacement D

An additional check is to compare measured and computed force-displacement relationships. Experimental data using different sphere radii: 11.8, 15.1, 18.4 and 21.7 μm are compared with our FE results in Fig. 6. Fig. 6 shows good agreement between the experiments and our simulations. Deviation from experiments starts to occur near the maximum force, which corresponds to rapid shrinkage of the contact line followed by detachment. The *FE* results show that, to a good approximation, there is a linear relationship between the force and displacement before instability occurs, which is consistent with experiments.

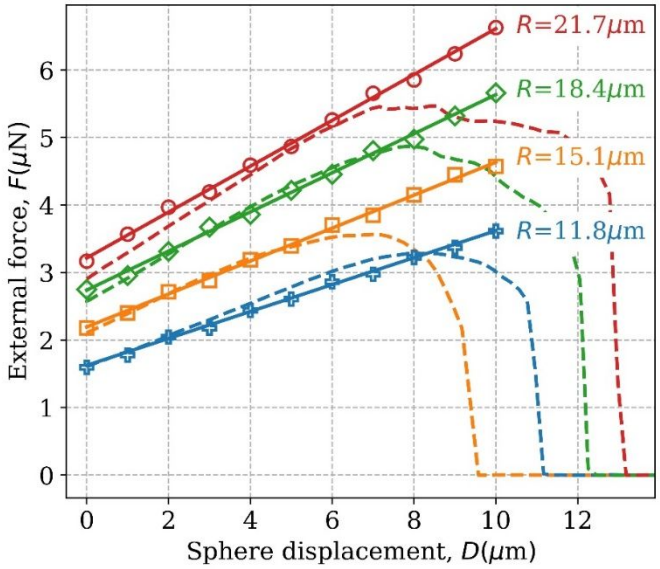

Fig. 6. External force F plotted versus sphere displacement D for different sphere radius. Finite element results are plotted as symbols, and the experimental results are plotted as dashed lines. The linear interpretations of FEM results (solid lines) suggest a linear relationship between indenter displacement and force.

3.3 Stress distribution in bulk elasticity on the surface and surface stress distribution

We use our simulation to estimate the contribution to the external force from surface stress and from elasticity, which is difficult to measure in experiments. The components of *true* stress in the substrate in the *r*-*z* plane are denoted by σ_{rr}, σ_{zz} and σ_{rz}. These stresses are evaluated on the substrate surface, both inside and outside the contact region. Results are shown in Fig. 7 and Fig. 8 for the case of a sphere with radius of 11.8μm. Fig. 7 shows that the stresses σ_{rr} and σ_{zz} reach their peaks at the contact line, dropping rapidly over a short distance near the contact line, and finally decay to a small value. The shear stress σ_{rz} is almost zero and negligible in the contact region. As the displacement increases, σ_{zz} increases while σ_{rz} remains very small in the contact region. It is interesting to note that part of the contact always remains under compressive stress despite the fact that $D > 0$. However, comparison of Fig. 7a and b shows that this region of compression decreases with increasing D, as expected. In our simulations, we found that for sufficiently large D, the contact region will be under tension.

The bulk elasticity contribution to the retraction force is determined by integrating the normal true traction in the bulk over the contact region,

$$F_{\text{elastic}} = \int_A t_z \, dA = \int_A \left(\sigma_{rz} n_r + \sigma_{zz} n_z \right) dA \tag{7}$$

where t_z is the component of traction in the z-direction, and n_r and n_z are the components of the unit normal vector to contact region in the r- and z-directions, respectively. As shown in Fig. 8, the external force is borne almost entirely by the surface stress in the beginning of the experiment, where the applied force is relatively small. For this case, elasticity's contribution to resisting deformation is small. This result is consistent with the theory, for sufficiently small spheres, the force due to surface stress and the applied force are in static equilibrium – they form a Neumann triangle of forces. However, as the sphere displacement D increases, bulk elasticity comes into play, and the ratio of the contributions from bulk elasticity to surface stress increases. One should expect that elasticity will play a stronger role for larger spheres. Theoretical results based on a *constant* isotropic surface stress model[13,15,16,38] suggest that whether or not elasticity dominates depends on a single dimensionless parameter

$\omega = \dfrac{\sigma_0}{(\mu R)^{2/3}\left[9\pi W_{ad}/4\right]^{1/3}}$ where W_{ad} is the work of adhesion between the sphere and the substrate. A small ω corresponds to the *JKR* limit where elasticity dominates. This limit corresponds to small surface tension, large spheres or stiff substrates. In the experiments of Jensen et al.[32] the maximum sphere radius is 21.7 μm. In the Electronic Supplementary Information, we compute the contribution of elasticity to the retraction force for this case and do find a small increase in the contribution due to elasticity. However, it is important to note that the use of ω relies on a constant surface stress, whereas in our case the surface hardens substantially, so surface stress indeed dominates elasticity in these experiments.

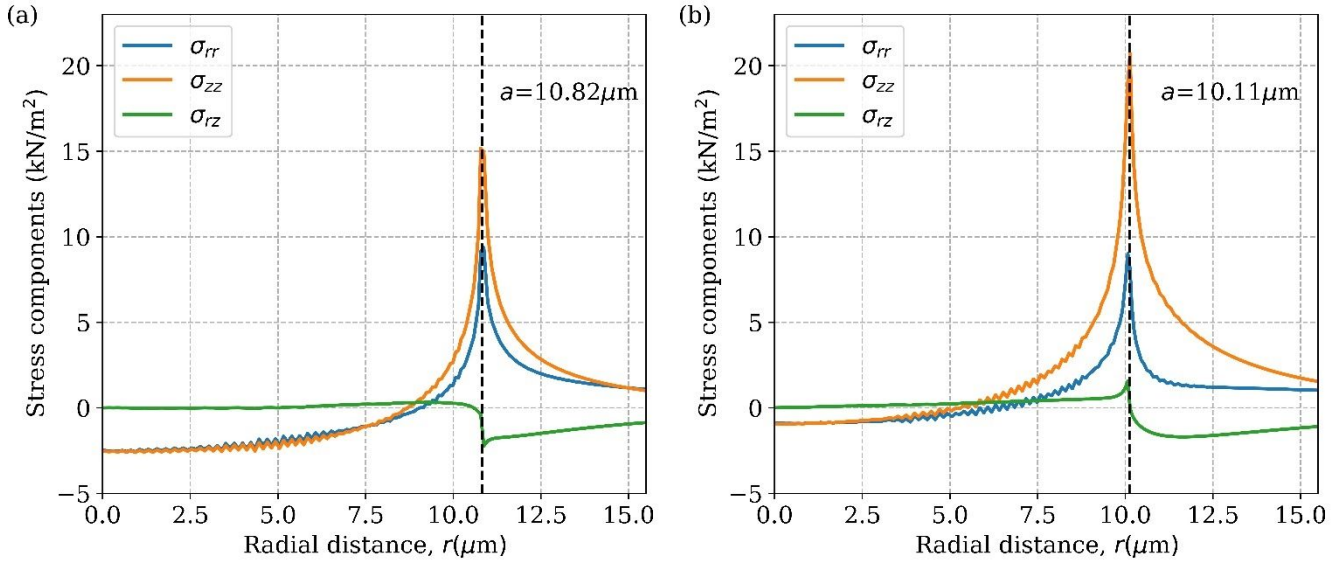

Fig. 7. Stress components plotted versus radial distance using a 11.8-μm-radius sphere (a) D=0 μm; (b) D=8 μm. Stress components of σ_{rr}, σ_{zz} and σ_{rz} are plotted as solid blue, orange and green lines respectively. The vertical black dashed lines indicate the contact radii at given imposed sphere displacements. In both (a) and (b), the region inside the contact is to the left of the vertical dotted line.

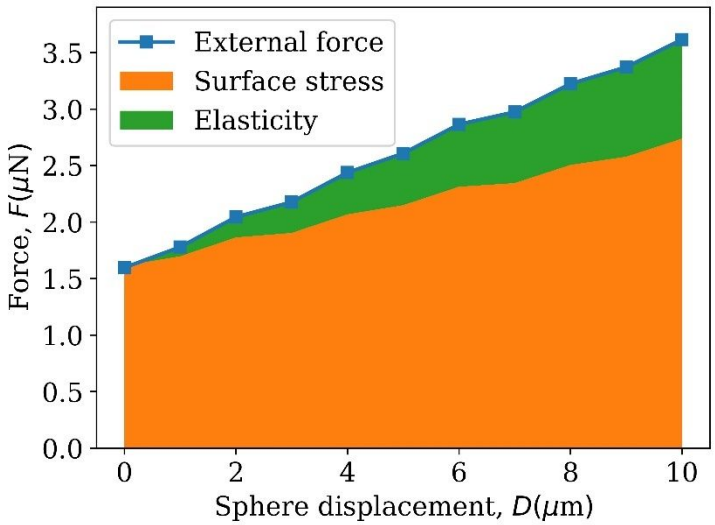

Fig. 8. Contribution to the total external force from surface stress (orange stacked area) and from elasticity (green stacked area) versus sphere displacement, using an 11.8-μm-radius sphere. Ratio of the contributions from bulk elasticity to surface stress increases as the sphere displacement increases and resistance from bulk elasticity is no longer negligible.

Finally, we plot the magnitude of surface stress versus the arc length measured from the contact line, i.e., $s = 0$ in Fig. 9. It demonstrates that the surface stress increases dramatically as the contact line is approached.

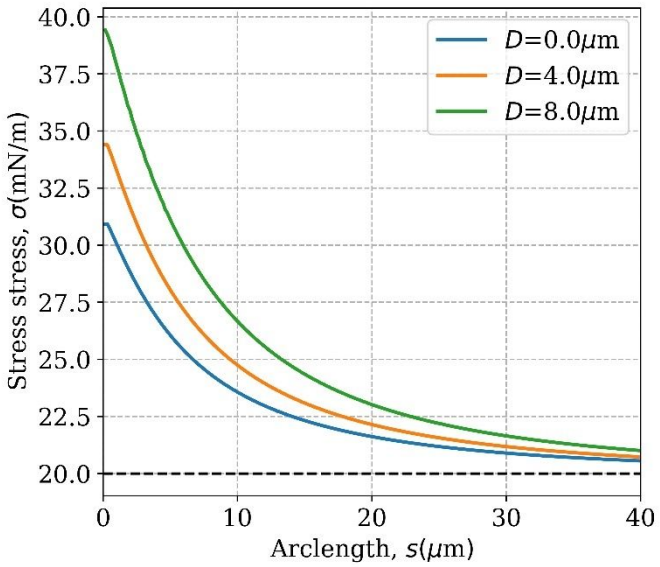

Fig. 9. Surface stress versus arc length measured from the contact line using a 11.8-μm-radius sphere. Solid blue, orange and green lines represent different cases with sphere displacements D=0, 4 and 8 μm respectively, and dashed black line represents the surface stress at no stretch for comparison.

4 Discussion

Our model based on the eq. (5) does remarkably well for capturing the relation between force and displacement observed in experiments. This result lends support to the very large surface strain stiffening effect observed by Xu et al.[25,31] However, we notice a discrepancy between the experimental surface profiles (dashed blue line) and FE simulation (solid orange line), as shown in Fig. 10. In the experiments, the contact line is almost tangent to the sphere, suggesting total wetting. Also, in the simulations we do not have a region of constant mean curvature near the contact line which is observed in experiments.

A possible way to capture this local total wetting phenomenon is to use a different model which involves bi-material and bi-surface-stress behaviors. In this model, which we labeled as FE 2, the bulk material near the contact line is assumed to be fluid like, with a very small Young modulus, E_c (see Fig. 11 for a schematic). Also, the surface stress in this region is assumed to be isotropic and insensitive to surface strain and has magnitude σ_0. Away from this region, the surface stress is modeled by eq. (5) and the bulk property is modeled by (6). We then simulate the retraction process using this new model. In the simulation, the σ_0 in both regions are identical and is the same as FE 1 (the model we have used throughout this work), while the modulus E_c is used as an adjustable parameter to fit the experimental surface profile. This fit (FE 2) is plotted in Fig. 10. The fitted surface profile (solid green line) agrees reasonably well with experiment where there is a region of constant mean curvature region (dashed red lines). However, this model will underestimate the force versus displacement, as shown in the Electronic Supplementary Information. In other words, the force predicted by a model with fluid like behavior near the contact line is inconsistent with the experimental data. Although model FE1 struggles to reproduce the experimental surface geometry, it does a much better job reproducing the forces of soft adhesion than other models. Significant further work will be required to reconcile the difference in geometry.

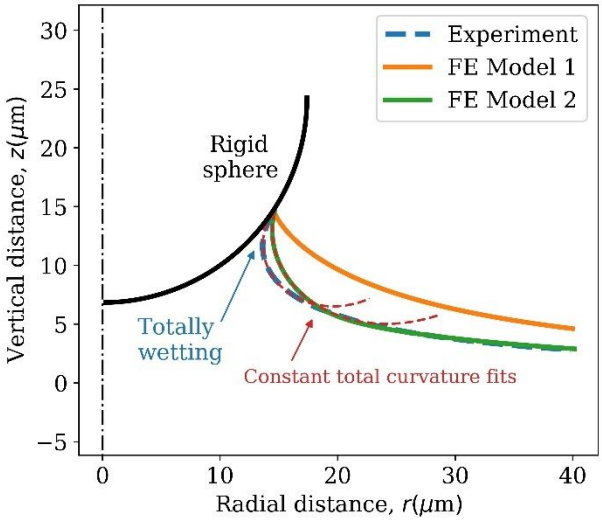

Fig. 10. Surface profiles for a 17.4-μm-radius sphere extracted from experimental data (dashed line) and finite element results (solid orange and green lines for FE model 1 and FE model 2, respectively). The experimental surface profile indicates the totally wetting phenomenon near the contact line. Constant total curvature fits (dashed red lines) are overlaid on the surface profiles.

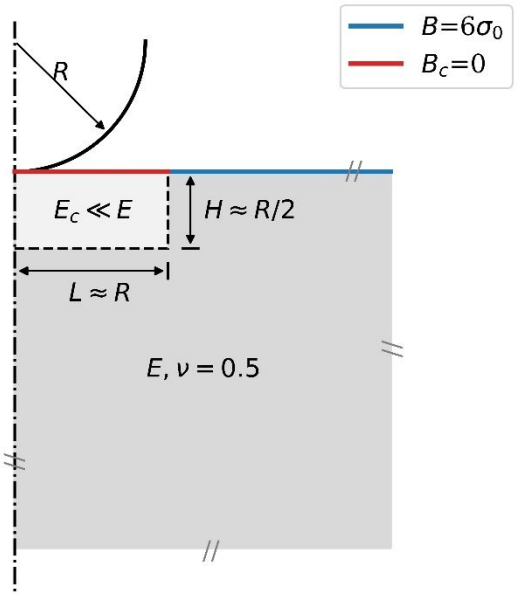

Fig. 11. Bi-material and bi-surface-stress finite element model. The light gray region represents the near-field structure with an extremely low Young's modulus; and surface stress is constant inside the dotted region and is strain dependent outside.

There is another possibility: the absence of a constant mean curvature region near the contact line can be due to a surface stress that is non-isotropic, as reported recently.[25,31] We also carried out simulations using a surface stress model of the form where the surface energy density function W allows for surface shear. The surface moduli in these calculations are chosen so that when the surface is subjected to an equiaxial state of stress, the surface stresses are consistent with the isotropic surface model in eq. (5). As mentioned earlier, axi-symmetry in this problem disallows surface shear strain/stress but *does* allow a bi-axial surface stress state. However, the surface profiles in these simulations do not show a region of constant mean curvature and are practically identical to the surface profiles obtained using the isotropic surface model eq. (5). Details of these simulations can be found in the Electronic Supplementary Information.

An anonymous reviewer suggested that perhaps strain hardening of the gel can contribute to this discrepancy. This reviewer has observed that the stress state in Fig.7b is close to be hydrostatic, with magnitude about 4 times the Young's modulus of the gel. However, in an incompressible solid, hydrostatic stress has no effect on deformation - the *maximum* principal stretch ratio in our simulations at the contact line is actually quite moderate, less than 2.7 for the case of $D = 8$ microns; therefore, one expects the neo-Hookean model should give a reasonable representation of the material behavior in this regime. This is certainly the case for elastomerd (see Fig. 2 of Boyce and Arruda[39]) where the neo-Hookean model gives a good approximation to the nominal stress versus stretch behavior for extension ratios less than 3. Indeed, a typical elastomer subjected to simple tension will strain softens slightly at a stretch ratio of around 2.5, then hardens at stretch ratio of 5 to 6 – well beyond the maximum stretch we observed in our simulations. As a further check, we carried out one simulation (sphere radius R=11.8, sphere displacement $D = 8$ microns) using a constitutive model (Yeoh solid) that allows for strain hardening. The strain energy density function W of the Yeoh solid is

$$W = \sum_{k=1}^{3} C_k \left(I_1 - 3\right)^k \quad , \tag{8}$$

where the C_k's are material parameters with units of stress, I_1 is the trace of the right Cauchy-Green tensor and k controls the amount of strain hardening. In this model $C_1 = \mu/2$ where μ is the small strain shear modulus. It should be noted that the neo-Hookean model is a special case of the Yeoh model with $C_2 = C_3 = 0$. We use the same small strain shear modulus and surface model in this simulation, and set $C_2 / C_1 = -0.005$, $C_2 / C_3 = 0.0001$. The choice of these parameters and details are given in the Electronic Supplementary Information. As expected, we do not find any difference between the surface profiles as well as the stress distribution at the contact line. Therefore, we believe that strain hardening is not the reason why the meniscus shape could not be captured.

The experiments and theory both indicate that force is linearly related to the displacement during retraction as long as the contact is *fixed*. This has to be the case for small deformation and a linear elastic material since the geometry is *fixed*. Indeed, for JKR theory, the relationship between force F and displacement D at fixed contact radius a is given by

$$D - D_0 = \frac{F - F_0}{8\mu a} \tag{9}$$

where D_0 and F_0 are the initial displacement and force, respectively. The quantity $1/8\mu a$ is the compliance of a rigid cylindrical punch of radius a bonded to an infinite block of incompressible elastic substrate. For an incompressible elastic substrate with a constant isotropic surface stress, eq. (9) is modified to

$$D - D_0 = \frac{\phi\left(\sigma_0 / 2\mu a\right)}{8\mu a}\left[F - F_0\right]. \tag{10}$$

The dimensionless function ϕ depends only on the Elasto-capillary number and is given by (3.20a) in Hui et al.[13] What is surprising is that this *linear* relation remains valid for large deformation as demonstrated by Liu et al.[9] For our case the solution is more complicated, since the compliance also depend on the ratio of stiffening coefficient B and σ_0. We have not been able to obtain a simple expression for this compliance. Nevertheless, our finite element method can be used to determine this relation for any given B and σ_0. In experiments, the elastic modulus, the contact radius, the displacement and force can be readily obtained. Thus, B and σ_0 can be determined by matching simulation results to force versus displacement data.

5 Conclusions

We have shown that strain-dependent surface stresses can provide a dominant contribution to the force-displacement curve of a rigid spherical contact on a compliant substrate. These findings corroborate the interpretation of recent experiments by Jensen et al.[32] and raise a number of important issues and opportunities. From an applications perspective, they suggest an exciting new design space for engineering soft adhesive contacts with tunable surface stresses. They also indicate that new design rules may be needed for these materials. In particular, the simple linear force-displacement relationship observed in both the experiments and our simulations calls for a parametric study to reveal the dependence of the contact stiffness on material properties and contact geometry.

In the shorter term, significant challenges remain in the reconciliation of theory and simple experiments, especially regarding the geometry of the contact and substrate deformation. It is natural to hypothesize that the capillary-bridge shape of the contact zone could actually be comprised of solvent extracted from the gel, but other previous observations contradict this hypothesis. Phase separation of solvent around an adhesive contact in the same material system was thoroughly investigated in Jensen et al.[40] There, the volume of phase-separated solvent was found to increase with the volume of indentation, suggesting that there should be no phase separation under net tension, investigated here. Further, the dynamics of the failure of the adhesive contacts in this same system was recently described in Berman et al.[33] In that study, the failure of the contact and the relaxation of the substrate was found to be distinctly solid-like, with no suggestion of a role for phase-separated fluid in a stretched adhesive contact.

It is possible that the discrepancy between the observed and calculated substrate surface deformations may arise from ambiguities in the contact conditions at the sphere-substrate interface. For one, there are no experimental measurements of how the substrate deforms during the establishment of contact that could be compared to the numerical protocol shown in Fig. 4. Additionally, the existing calculation does not impose a boundary condition for the contact angle at the three-phase contact line. While such a boundary condition has been suggested by several works,[11,41,42] its form is not established, and consequently the simulations lack an appropriate contact line condition. Both of these considerations will be the subject of further experimental and theoretical study.

Conflicts of interest

There are no conflicts to declare.

Acknowledgement

The contributions of ZL, CYH, and AJ were supported by the U.S. Department of Energy, Office of Basic Energy Sciences, Division of Materials Sciences and Engineering under award DEFG02-07ER46463. We thank an anonymous reviewer for the suggestion that the discrepancy between theory and experiment could be due to strain hardening of the gel.

References

1 R. Shuttleworth, *Proceedings of the Physical Society. Section A*, 1950, **63**, 444.
2 C. Y. Hui, A. Jagota, Y. Y. Lin and E. J. Kramer, *Langmuir*, 2002, **18**, 1394–1407.

3 R. W. Style, A. Jagota, C.-Y. Hui and E. R. Dufresne, *Annual Review of Condensed Matter Physics*, 2017, **8**, 99–118.
4 P.-G. de Gennes, F. Brochard-Wyart and D. Quéré, *Capillarity and wetting phenomena: drops, bubbles, pearls, waves*, Springer, New York, NY, 2010.
5 A. Jagota, D. Paretkar and A. Ghatak, *Phys. Rev. E*, 2012, **85**, 051602.
6 D. Paretkar, X. Xu, C.-Y. Hui and A. Jagota, *Soft Matter*, 2014, **10**, 4084–4090.
7 S. Mora, C. Maurini, T. Phou, J.-M. Fromental, B. Audoly and Y. Pomeau, *Phys. Rev. Lett.*, 2013, **111**, 114301.
8 A. Marchand, S. Das, J. H. Snoeijer and B. Andreotti, *Phys. Rev. Lett.*, 2012, **108**, 094301.
9 T. Liu, A. Jagota and C.-Y. Hui, *Extreme Mechanics Letters*, 2016, **9**, 310–316.
10 X. Xu, A. Jagota and C.-Y. Hui, *Soft Matter*, 2014, **10**, 4625–4632.
11 R. W. Style, C. Hyland, R. Boltyanskiy, J. S. Wettlaufer and E. R. Dufresne, *Nature Communications*, 2013, **4**, 2728.
12 K. L. Johnson, *Contact mechanics*, Cambridge University Press, Cambridge, 1985.
13 C.-Y. Hui, T. Liu, T. Salez, E. Raphael and A. Jagota, *Proceedings of the Royal Society A: Mathematical, Physical and Engineering Sciences*, 2015, **471**, 20140727–20140727.
14 Z. Cao, M. J. Stevens and A. V. Dobrynin, *Macromolecules*, 2014, **47**, 3203–3209.
15 J.-M. Y. Carrillo and A. V. Dobrynin, *Langmuir*, 2012, **28**, 10881–10890.
16 T. Salez, M. Benzaquen and É. Raphaël, *Soft Matter*, 2013, **9**, 10699.
17 C.-Y. Hui and A. Jagota, *Soft Matter*, 2015, **11**, 8960–8967.
18 E. R. Jerison, Y. Xu, L. A. Wilen and E. R. Dufresne, *Phys. Rev. Lett.*, 2011, **106**, 186103.
19 R. W. Style, R. Boltyanskiy, Y. Che, J. S. Wettlaufer, L. A. Wilen and E. R. Dufresne, *Phys. Rev. Lett.*, 2013, **110**, 066103.
20 A. Marchand, S. Das, J. H. Snoeijer and B. Andreotti, *Physical Review Letters*, 2012, **109**, 236101.
21 N. Nadermann, C.-Y. Hui and A. Jagota, *Proceedings of the National Academy of Sciences*, 2013, **110**, 10541–10545.
22 X. Xu, A. Jagota, D. Paretkar and C.-Y. Hui, *Soft Matter*, 2016, **12**, 5121–5126.
23 S. Mondal, M. Phukan and A. Ghatak, *Proceedings of the National Academy of Sciences*, 2015, **112**, 12563–12568.
24 D. Vella, M. Adda-Bedia and E. Cerda, *Soft Matter*, 2010, **6**, 5778.
25 Q. Xu, R. W. Style and E. R. Dufresne, *Soft Matter*, 2018, **14**, 916–920.
26 R. W. Style, R. Boltyanskiy, B. Allen, K. E. Jensen, H. P. Foote, J. S. Wettlaufer and E. R. Dufresne, *Nature Physics*, 2014, **11**, 82–87.
27 R. C. Cammarata and K. Sieradzki, *Annual Review of Materials Science*, 1994, **24**, 215–234.
28 H. Wu, Z. Liu, A. Jagota and C.-Y. Hui, *Soft Matter*, 2018, **14**, 1847–1855.
29 R. W. Style and Q. Xu, *Soft Matter*, 2018, **14**, 4569–4576.
30 M. E. Gurtin and A. Ian Murdoch, *International Journal of Solids and Structures*, 1978, **14**, 431–440.
31 Q. Xu, K. E. Jensen, R. Boltyanskiy, R. Sarfati, R. W. Style and E. R. Dufresne, *Nature Communications*, 2017, **8**, 555.
32 K. E. Jensen, R. W. Style, Q. Xu and E. R. Dufresne, *Physical Review X*, 2017, **7**, 041031.
33 J. D. Berman, M. Randeria, R. Style, Q. Xu, J. R. Nichols, A. J. Duncan, M. Loewenberg, E. Dufresne and K. E. Jensen, *Soft Matter*, 2019.
34 D. Maugis, *Langmuir*, 1995, **11**, 679–682.
35 Y.-Y. Lin and H.-Y. Chen, *Journal of Polymer Science Part B: Polymer Physics*, 2006, **44**, 2912–2922.
36 A. E. Green, P. M. Naghdi and W. L. Wainwright, *Archive for Rational Mechanics and Analysis*, 1965, **20**, 287–308.
37 D. J. Steigmann and R. W. Ogden, *Proceedings of the Royal Society of London. Series A: Mathematical, Physical and Engineering Sciences*, 1999, **455**, 437.
38 Z. Cao, M. J. Stevens and A. V. Dobrynin, *Macromolecules*, 2014, **47**, 6515–6521.
39 M. C. Boyce and E. M. Arruda, *Rubber Chemistry and Technology*, 2000, **73**, 504–523.
40 K. E. Jensen, R. Sarfati, R. W. Style, R. Boltyanskiy, A. Chakrabarti, M. K. Chaudhury and E. R. Dufresne, *Proceedings of the National Academy of Sciences*, 2015, **112**, 14490–14494.

41 C.-Y. Hui and A. Jagota, *Proceedings of the Royal Society A: Mathematical, Physical and Engineering Sciences*, 2014, **470**, 20140085–20140085.
42 S. Karpitschka, L. van Wijngaarden and J. H. Snoeijer, *Soft Matter*, 2016, **12**, 4463–4471.